ACS APPLIED MATERIALS & INTERFACES

Research Article

www.acsami.org

Modulation of Endothelial Cell Migration via Manipulation of Adhesion Site Growth Using Nanopatterned Surfaces

John H. Slater,*,ψ Patrick J. Boyce, Matthew P. Jancaitis, Harold E. Gaubert, Alex L. Chang, Mia K. Markey, and Wolfgang Frey

Department of Biomedical Engineering, University of Texas, Austin, Texas 78712, United States

Supporting Information

ABSTRACT: Orthogonally functionalized nanopatterend surfaces presenting discrete domains of fibronectin ranging from 92 to 405 nm were implemented to investigate the influence of limiting adhesion site growth on cell migration. We demonstrate that limiting adhesion site growth to small, immature adhesions using sub-100 nm patterns induced cells to form a significantly increased number of smaller, more densely packed adhesions that displayed few interactions with actin stress fibers. Human umbilical vein endothelial cells exhibiting these traits displayed highly dynamic fluctuations in spreading and a 4.8-fold increase in speed compared to cells on nonpatterned controls. As adhesions were allowed to mature in size in cells cultured on larger nanopatterns, 222 to 405 nm, the dynamic fluctuations in spread area and migration began to slow, yet cells still displayed a 2.1-fold increase in speed compared to controls. As all restrictions on adhesion site growth were lifted using nonpatterned controls, cells formed significantly fewer, less densely packed, larger, mature adhesions that acted as terminating sites for actin stress fibers and significantly slower migration. The results revealed an exponential decay in cell speed with increased adhesion site size, indicating that preventing the formation of large mature adhesions may disrupt cell stability thereby inducing highly migratory behavior.

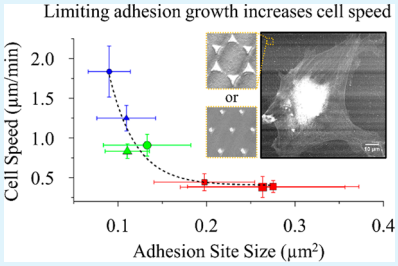

KEYWORDS: *nanopatterning, cell adhesion, cell migration, adhesion maturation, cell dynamics*

1. INTRODUCTION

Cell migration is a highly coordinated, multistep mechanochemical process that involves membrane extension at the leading edge, the generation of traction force to propel the cell forward, sustained application of traction for stabilization, cell translocation, and adhesion site disassembly.[1] Cellular adhesion to the extracellular matrix (ECM) plays a key role in each step of this process. These adhesions are mediated by integrins: heterodimeric transmembrane glycoproteins consisting of two subunits that combine to recognize specific peptide sequences in ECM proteins.[2] Upon activation, integrins cluster into small plaques ranging from tens to hundreds of nanometers that act as an initiation site for adhesion formation.[3] These small clusters can develop into nascent adhesions, ≤0.19 μm^2, at the leading edge of lamellapodia that are responsible for the generation of strong traction forces, through their interaction with treadmilling actin, that propel the cell forward.[4] These short-lived adhesions, with a lifetime on the order of 1 min, are either disassembled[5] or begin associating with actin stress fibers to undergo force-mediated maturation.[6] As the sustained application of force proceeds through Rho-mediated actomyosin contraction, these small, immature adhesions grow to ∼0.25−0.38 μm^2, increase in molecular diversity, and mature into focal complexes.[6,7] Focal complexes continue applying traction through their interactions with small actin stress fibers and can either be disassembled[5] or continue to grow and become fully mature focal adhesions. Mature focal adhesions, ∼1−10 μm^2, act as terminating sites for actin stress fibers, thereby providing stability to the cell.[6,7] These stabilizing adhesions often remain stationary as the cell translocates and eventually end up at the rear of the cell where they are disassembled. The lifetime of focal adhesions ranges from 8.5 min[8] to 47 min,[9] and it has been demonstrated that adhesion site disassembly can be a rate-limiting step in migration.[5,9,10]

Knowing that small, immature adhesions apply substantial[4,11] short-lived[12] traction forces,[4,13,14] that these adhesions can undergo force-mediated maturation[12] to become mature focal adhesions,[7] and that disassembly of mature adhesions can be a rate-limiting step in migration,[10,15,16] one may hypothesize that preventing adhesion site growth, and with it maturation, could abolish the formation of large stabilizing adhesions resulting in increased migratory behavior.

To investigate the influence of limiting adhesion site growth on cell migration, it is imperative that the patterned surfaces provide discrete nanosized domains of an adhesive ligand against a nonadhesive background in the size regime associated with various levels of adhesion maturation, ≤0.19 μm^2, for nascent adhesions,[4] and ∼0.25−0.38 μm^2 for focal complexes[6,7] which correspond to circular patterns with diameters of 492 nm and ∼564−696 nm, respectively. Reported sizes of immature adhesions were measured via fluorescent microscopy and are near the resolution limits of light microscopy, particularly for

Received: December 18, 2014
Accepted: January 27, 2015
Published: January 27, 2015

DOI: 10.1021/am508906f
ACS Appl. Mater. Interfaces 2015, 7, 4390−4400

nascent adhesions. Super-resolution imaging of live cells has demonstrated nanosized adhesions with dimensions of ∼120 nm (0.01 μm^2).[17] While many studies concerning cell migration on micropatterned surfaces exist[18−23] it is difficult to create nanopatterns over large surface areas needed for cell migration experiments using traditional photolithography. Although some techniques such as electron beam lithography allow for high resolution patterning they are serial in nature and therefore time-consuming to produce the surface area needed. Alternatively, parallel methods based on self-assembly allow for the fabrication of nanopatterns over large surface areas and have been implemented to investigate the influences of ligand density, integrin spacing, and adhesion site size on cell adhesion, spreading, and proliferation.[24−33] Relatively few studies have implemented nanopatterned surfaces to investigate the influence of limiting adhesion site growth on cell migration, particularly in the <0.1 μm^2 size regime.

Toward this goal, it has been demonstrated that adhesion maturation is impaired in cells cultured on patterns smaller than 500 nm and that the formation of fully mature focal adhesions begins to occur when adhesion sites reach a size of ∼1 μm^2.[32,34,35] When adhesion site maturation is halted, cells are typically less spread, form fewer actin stress fibers, and display increased lamellipodia or filopodia.[32,34,36] While these trends have been observed in a number of studies, the influence of limiting adhesion growth on cell migration may be cell type or ligand dependent. Swiss albino 3T3 fibroblasts displayed a 4-fold increase in migration when cultured on 500 nm fibronectin (FN) patterns compared to cells on nonpatterned controls.[36] Conversely, immortalized mouse embryonic kidney fibroblasts cultured on 500 nm patterns displaying the adhesive peptide RGD exhibited a 3-fold decrease in migration compared to those on 2 μm patterns.[34] These discrepancies in migration rates may stem from differences in integrin usage based on ECM composition or potentially on cell type.

To gain a better understanding of how limiting adhesion site growth can influence cell migration, we implemented Nano-Sphere Lithography (NSL) in combination with an orthogonal surface functionalization scheme to produce surfaces displaying discrete nanodomains of FN against a biologically inert background that provided modulation of adhesion site size by varying nanopattern size. We demonstrate that limiting adhesion site growth to small, immature adhesions using sub-100 nm sized FN patterns induced an altered cellular adhesive state characterized by a significant increase in smaller, more densely packed adhesions that displayed very few interactions with actin stress fibers indicative of nascent adhesions or very small focal complexes. Limiting adhesion site growth to this regime induced highly migratory cell behavior characterized by a 4.8-fold increase in cell speed that was accompanied by dynamic fluctuations in spread area and a significantly higher random motility coefficient. As the nanopatterns increased to 222 to 405 nm cells exhibited a change in their adhesive state and formed fewer but larger adhesions. These adhesions displayed increased interactions with actin stress fibers and were on the size regime indicative of focal complexes. Cells exhibiting these adhesive properties displayed decreased migration compared to cells on sub-100 nm sized patterns but still exhibited a 2.1-fold higher speed compared to cells on nonpatterned controls. Cells on control surfaces, where all restrictions on adhesion site growth were abolished, displayed large mature adhesions at the tips of actin stress fibers with a distinct peripheral location indicative of mature focal adhesions. Consequently, these cells exhibited the slowest migration. These results indicate that limiting adhesion site growth may induce highly migratory cell behavior by decreasing cell stability.

2. MATERIALS AND METHODS

2.1. Surface Preparation. The nanopatterned surfaces were fabricated, functionalized, and characterized as previously reported.[31] Briefly, glass slides (Erie Scientific Company, Portsmouth, NH) were piranha cleaned and coated with a mono- or bilayer of polystyrene spheres (Duke Scientific, Fremont, CA). Two nanometers of chromium (R.D. Mathis, Long Beach, CA) and 8 nm of gold (Alfa Aesar, Ward Hill, MA) were thermally evaporated onto the surfaces (Denton Vacuum, Moorestown, NJ), the spheres removed, the surfaces exposed to an air plasma and immersed in a 26.5 mM hydrochloric acid (Fisher Scientific, Pittsburgh, PA), 1 mM hexadecanethiol (HDT) (Aldrich, St. Louis, MO), and 41 mM 2-methoxy(polyethyleneoxy)-propyltrimethoxysilane (OEG-silane) (Gelest, Morrisville, PA) solution in toluene (Fisher Scientific, Pittsburgh, PA) for 48 h with continuous stirring. The samples were rinsed, dried with nitrogen (N_2), and baked at 105 °C for 1 h. The functionalized nanopatterned surfaces were exposed to 3 mL of human plasma fibronectin (Sigma, St. Louis, MO) at a concentration of 10 μg/mL in 50 mM HEPES for 20 min. Control surfaces with varying FN surface densities were created by functionalizing Au surfaces with a 1 mM ethanolic solution of HDT overnight followed by exposure to FN at concentrations of 2, 10, or 25 μg/mL in 50 mM HEPES for 20 min. The protein adsorbed surfaces were rinsed twice with HEPES, and cells were immediately seeded. Surfaces were characterized with atomic force microscopy (AFM), fluorescence microscopy, and X-ray photoelectron spectroscopy (XPS) as previously described.[31]

2.2. Cells and Reagents. Nonpooled human umbilical vein endothelial cells (HUVECs), passages 2−4, were cultured in endothelial growth media (EGM) supplemented with 2 mL of bovine brain extract, 0.5 mL of human endothelial growth factor, 0.5 mL of hydrocortisone, 0.5 mL of gentamicin/amphotericin-B, and 10 mL of fetal bovine serum according to the supplier's instructions (all reagents and cells: Lonza Group Ltd., Basel, Switzerland). The cells were cultured at 37 °C and 5% CO_2 to 90% confluence in T-25 tissue culture flasks coated with 30 μg of FN. The cells were trypsinized with 3.0 mL of 0.25% trypsin and 1 mM ethylenediaminotetraacetic acid in PBS at 37 °C for 5 min. The cells were collected and centrifuged, and the cell pellet was resuspended in full EGM media and sparsely seeded at a density of ∼10 cells/mm^2 to minimize cell−cell contact.

2.3. Fluorescent Labeling and Imaging of Fibronectin, Vinculin, and Actin. After 24 or 72 h of culture, the samples were rinsed with 25 mL of warm phosphate-buffered saline supplemented with 0.02% Tween 20 (PBS-T) and immediately immersed into a modified, ice-cold cytoskeleton stabilizing buffer (CSK) (10 mM HEPES, 0.5% Triton X-100, 300 mM sucrose, 3 mM $MgCl_2$, and 50 mM NaCl, pH 6.8 in DI H_2O) for 1 min. The samples were removed from the CSK and immediately submersed into ice-cold 5% formaldehyde in PBS-T and placed in a 37 °C water bath for 10 min. The samples were rinsed with 25 mL of warm PBS-T followed by blocking solution with 1% BSA in PBS (PBSA) for 20 min. The cells were labeled with a tristain solution [1:50 dilution of FITC-conjugated monoclonal antivinculin (Sigma Chemicals, St. Louis, MO), 1:1100 dilution of Rhodamine-phalloidin (Sigma Chemicals, St. Louis, MO), and 1:550 dilution of rabbit antifibronectin (Abcam, Cambridge, MA) in PBS supplemented with 0.02% Tween 20 and 1% BSA (PBSA-T)] overnight at 4 °C. The samples were rinsed with PBS-T and washed in 0.1% Tween 20 in PBS for 20 min. The samples were exposed to a 1:500 dilution of marina blue conjugated goat antirabbit (Invitrogen, Eugene, OR) solution in PBSA-T for 1 h. The surfaces were thoroughly rinsed and washed in PBS-T for 20 min followed by a rinse in DI H_2O supplemented with 0.02% Tween 20 and dried with N_2. A drop of ProLong Gold antifade reagent (Molecular Probes, Inc., Eugene, OR) was added, and the samples were covered with a 24 by 60 mm coverslip and secured with clear fingernail polish. Fluorescent

DOI: 10.1021/am508906f
ACS Appl. Mater. Interfaces 2015, 7, 4390−4400

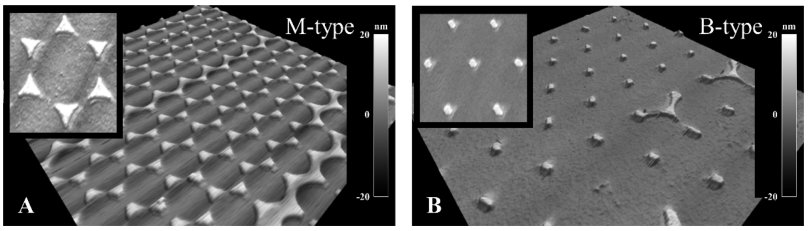

Figure 1. Properties of nanopatterned and control surfaces. (A, B) 3D AFM representations of (A) monolayer (M-type) and (B) bilayer (B-type) nanopatterned surfaces created with nanosphere lithography (NSL); insets display the base geometry that is arrayed over the surface. Table 1 displays the FN surface density for nanopatterned and control surfaces and the characteristic nanopattern size (bisector of the triangle for M-type and diameter of the spots for B-type), nanopattern area, center-to-center spacing, and (rim-to-rim spacing) for nanopatterned surfaces. The Au nanopatterns cover 7.2 ± 0.4 and 2.2 ± 0.4% of the surface for M- and B-type surfaces, respectively. The nomenclature for the nanopatterned surfaces is as follows: the number indicates the diameter of the spheres, in nm, and M or B indicates a monolayer or bilayer configuration. The nomenclature for the control surfaces indicates the solution concentration of FN to which they were exposed in μg/mL. The symbols to the left of the surface name are used in subsequent figures to indicate from which surface the data was acquired.

Table 1. Nanopatterned and Nonpatterned Control Surface Properties

Surface	FN Density (FN/μm^2)	Size (nm)	Area (μm^2)	Spacing (nm)
● 0300B	41	92 ± 33	0.004 ± 0.001	308 ± 11 [216]
▲ 0300M	217	94 ± 11	0.005 ± 0.001	177 ± 13 [83]
● 1500B	41	222 ± 25	0.047 ± 0.008	1,534 ± 19 [1,312]
▲ 1500M	217	405 ± 41	0.086 ± 0.017	883 ± 51 [478]
■ 02Au	537	---	---	---
■ 10Au	1,882	---	---	---
■ 25Au	2,474	---	---	---

images were acquired via optical sectioning using structured illumination on a Zeiss Axiovert 200 ApoTome (Carl Zeiss MicroImaging, Inc., Thornwood, NY) inverted microscope equipped with a Zeiss Axiocam MRm charge-coupled device camera (Carl Zeiss MicroImaging, Inc., Thornwood, NY) to eliminate fluorescence signal from other focal planes.

2.4. Image Processing. The raw fluorescent images were band-pass filtered with a Fast Fourier Transformation using ImageJ (NIH, Bethesda, MD) to increase the contrast between the labeled adhesions and background.[37] After filtration, the images were processed with an iterative threshold algorithm using Igor Pro 5 (WaveMetrics, Lake Oswego, OR) to create binary images for automated adhesion site analysis. Additional details are provided in Supporting Information.

2.5. Quantification of Fluorescently Labeled Vinculin-Containing Adhesions. The processed, binary images of fluorescently labeled adhesions were used to quantify the cell adhesive properties with an in-house developed algorithm written in ImageJ. The cells were outlined, and the *xy* coordinates for each pixel in the outline, the cell spreading area, and cell centroid were measured. The number of adhesions per cell, density of adhesions (number of adhesion sites per area), and adhesion site distribution were measured. Additional details are provided in Supporting Information.

2.6. Cell Migration Studies. After 24 h, the samples were placed on a Leica DM IRB (Leica Microsystems, Wetzlar Germany) inverted microscope equipped with an incubator that maintained the atmosphere at 37 °C and 5% CO_2. Time-lapse, phase-contrast microscopy was used to capture 15× magnification images of cells at 1 min intervals for 1.5 h using a Cooke Sensicam CCD camera (The Cooke Corporation, Romulus, Michigan) operated by Camware software (PCO Imaging, Kelheim, Germany). The time-lapse movies were recorded every 24 h for 3 days. The cell paths were manually tracked using a particle tracking plug-in in ImageJ (NIH, Bethesda, Maryland) created by Fabrice Cordelieres (Institut Curie, Orsay, France), and only cells that remained in the field of view, that did not make contacts with neighboring cells, and that did not undergo self-renewal were analyzed. An algorithm that corrected for sample drift during filming was implemented. The measured cell positions, in *xy* coordinates, were used to calculate the time-average mean square displacement, root-mean-square speed, total distance traveled, net distance traveled, persistence time, persistence length, and random motility coefficient (μ) as previously described.[38] Cell spread area versus time was analyzed by outlining the cells in each frame of the time-lapse movies with ImageJ. The area for each cell was normalized to the maximum spread area measured over the entire view time and plotted as a function of time.

2.7. Statistical Analysis. Statistical analysis was performed using SPSS 12.0 (SPSS, Chicago, IL). Data set distributions were tested for normality by evaluating the standard error of skewness and kurtosis. The calculated standard errors were between −2 and 2, thereby indicating normally distributed data. Levene's test for the equality of variances was performed to determine if equal variances could be assumed. The significance was greater than 0.1 and therefore equal variances were assumed. ANOVA with a post hoc Tukey test was implemented with a significance level of 0.05.

3. RESULTS

3.1. Surface Characterization. For nanopatterns to provide an upper limit to adhesion site growth it was imperative that the orthogonal functionalization scheme induced FN adsorption exclusively to the hexadecanethiol-functionalized gold (Au) nanopatterns while leaving the oligo(ethylene glycol)-silanized glass background free of protein. Using X-ray photoelectron microscopy (XPS) and atomic force microscopy (AFM), we previously demonstrated that FN adsorbed exclusively to the Au nanopatterns.[31] Since FN density is known to influence adhesion, spreading, and migration, we quantified the FN packing density on the patterns and determined that it was ∼714 FN/μm^2 regardless of pattern size, which we define as the local ligand density.[31] In contrast,

DOI: 10.1021/am508906f
ACS Appl. Mater. Interfaces 2015, 7, 4390−4400

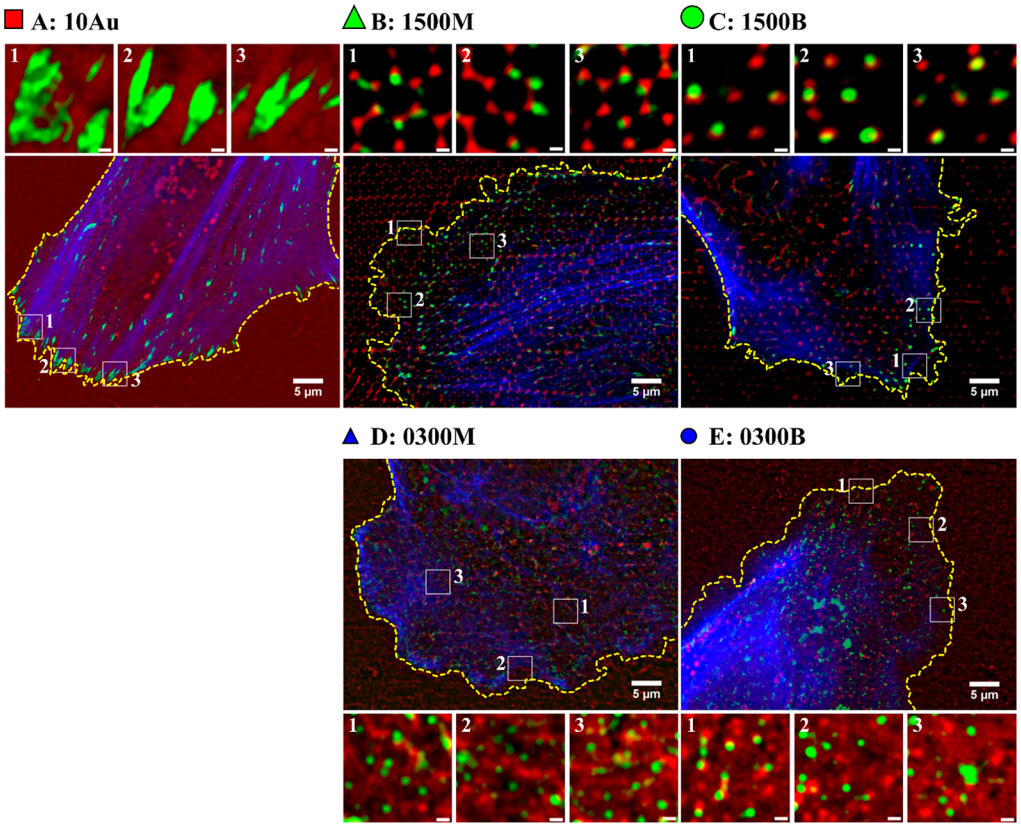

Figure 2. Nanopatterns limit adhesion site growth. (A–E) HUVECs were cultured on the indicated surface, fixed, and fluorescently immunolabeled for (red) fibronectin, (green) vinculin, and (blue) actin. The cell periphery is indicated by the dashed yellow line. (A) HUVECs cultured on nonpatterned controls formed large focal adhesions at the cell periphery (insets 1–3 in A) that were terminating sites for large actin stress fibers. (B–E) Adhesions formed by cells cultured on nanopatterned surfaces colocalized with the underlying FN nanopatterns (insets in B–E), and the extent of adhesion site growth was restricted by the nanopatterns (insets in B–E). As the nanopattern size decreased, the propensity for cells to form large actin stress fibers diminished and an actin meshwork composed of thin actin fibrils was observed. Inset scale bar = 500 nm. See Figure S1, Supporting Information, for an enlarged version.

the global ligand density, which takes both the Au patterns and surrounding inert background into account, was 41 and 217 FN/μm^2 for the B- and M-type surfaces, respectively, due to differences in pattern geometry (Figure 1). In this study, four nanopatterned surfaces were utilized with patterns ranging from 92 to 405 nm and pattern spacing from 177 nm to 1.534 μm (Table 1). Two surfaces displayed a global density of 41 FN/μm^2 with patterns of 92 nm (0.004 μm^2) and 222 nm (0.047 μm^2) for the 0300B and 1500B surfaces, respectively, and two displayed a global density of 217 FN/μm^2 with patterns of 94 nm (0.005 μm^2) and 405 nm (0.086 μm^2) for the 0300 and 1500 M surfaces, respectively (Table 1). To control for the influence of ligand density, we used nonpatterned, hexadecanethiol-functionalized Au surfaces displaying FN at 537, 1,882, and 2,474 FN/μm^2 as control surfaces (Table 1). Surface wettability influences the conformation of adsorbed FN which can influence integrin usage;[39−41] we avoided these influences by keeping the surface chemistry the same for both patterned and control surfaces.

3.2. Limiting Adhesion Site Growth with Nanopatterned Surfaces Induced an Increased Number of Smaller, More Densely Packed Adhesions and Prevented the Formation of Large Actin Stress Fibers. Human umbilical vein endothelial cells (HUVECs) were cultured on the functionalized nanopatterned surfaces, fixed, fluorescently immunolabeled for fibronectin (red), vinculin (green), and actin (blue), imaged with structured illumination, (Figure 2) and the adhesion site properties (size, number, density (number of adhesions per area), and distribution) quantified. The fluorescence signal from individual nanopatterns was optically resolved for all nanopatterns (red in insets Figure 2B–E) but more easily observed for larger patterns (red in insets Figure 2B,C). The FN nanopatterns provided an upper limit to adhesion site growth as indicated by colocalization of the FN (red) and vinculin (green) channels (insets in Figure 2B–E), but in some cases the adhesions appeared larger than the patterns. This could be due to pattern defects, close proximity of more than one adhesion site that could not be optically resolved, or bridging of adhesion components across multiple patterns[28] during fibrillogenesis. "Trails" of FN fibrils in the "wakes" of highly migratory cells on nanopatterned surfaces and very thin elongated adhesions were observed, indicating the ability to either remodel the patterned FN[31] or to integrate newly synthesized FN with the patterned FN. We observed that cells cultured on nanopatterned surfaces displayed smaller adhesions throughout the cell body, fewer actin stress fibers, and more distinct lamellipodia (Figure 2B–E) in contrast to cells on nonpatterned controls that displayed large adhesions mainly at their periphery that acted as terminating sites for actin stress fibers (Figure 2A).

Although we previously implemented combined fluorescent and atomic force microscopy for high-resolution imaging of very small adhesions (0.036–0.2 μm^2) formed by cells on nanopatterned surfaces,[31] this approach was too time-

DOI: 10.1021/am508906f
ACS Appl. Mater. Interfaces 2015, 7, 4390−4400

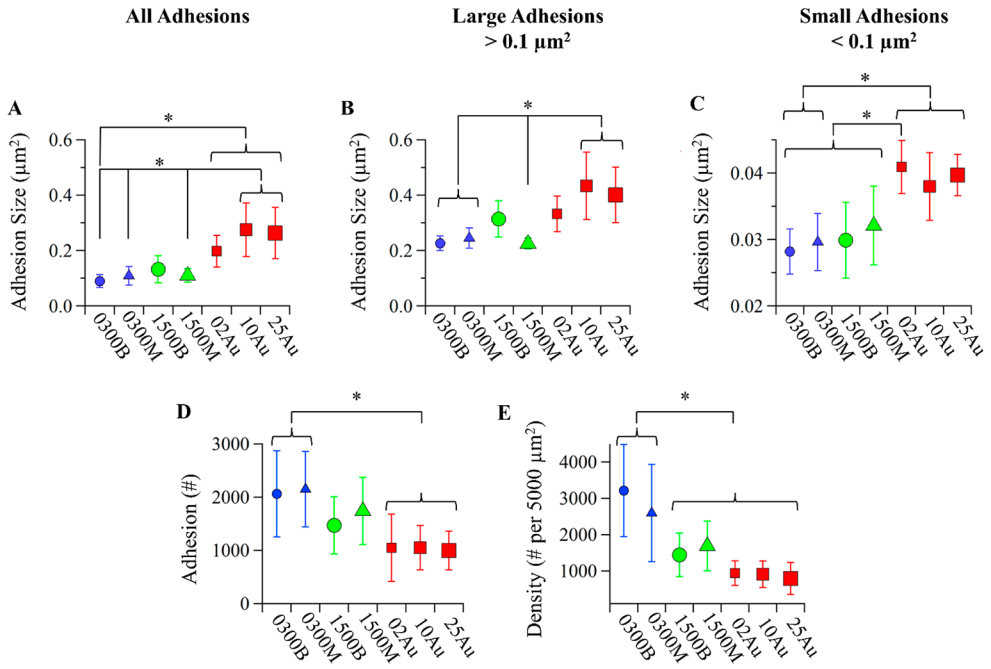

Figure 3. Limiting adhesion site growth with nanopatterned surfaces induces an increased number of more densely packed adhesions. Average (A–C) size, (D) number, and (E) density of vinculin-containing adhesions were measured from immunofluorescent images of HUVECs cultured on nanopatterned and control surfaces. (B, C) Due to resolution limitations of light microcopy, the measured size of adhesions smaller than 0.1 μm^2 was overestimated and the average adhesion site size for those (B) larger or (C) smaller than 0.1 μm^2 was determined independently. (A–C) Adhesion site growth was restricted in cells cultured on nanopatterned surfaces and was reflected in the significantly reduced adhesion site size compared to cells on nonpatterned controls. (D) Restricting adhesion site growth with sub-100 nm sized patterns induced HUVECs to form a significantly increased number of smaller adhesions that (E) were more densely packed compared to cells on control surfaces. * indicates $p < 0.5$.

consuming to be implemented on the large cell population needed for the work presented here so structured illumination was implemented. To better cope with optical resolution limitations, an image processing technique was developed that implemented a difference of gaussians transfer function and iterative thresholding for the detection and quantification of very small adhesions. Image processing allowed for accurate detection of adhesion sites over a broad range of sizes and accurate measurement of adhesion site size for adhesions larger than 0.10 μm^2. An investigation of the adhesion site size distribution demonstrated that the data were not normally distributed. Adhesions larger than 0.10 μm^2 displayed a log-normal distribution, while adhesions smaller than 0.10 μm^2 displayed an increase faster than log-normal, indicating the inability to accurately measure the size of adhesions smaller than 0.10 μm^2. Therefore, the number of adhesion sites formed could be accurately detected regardless of size but the measured size of adhesions, when smaller than 0.10 μm^2, was artificially enlarged. Studies concerning the quantification of cellular adhesions often implement a minimum cutoff of 0.25–0.56 μm^2.[42−44] While this prevents the incorporation of noise and background into the analysis and bypasses optical resolution issues, it also biases the results toward larger focal adhesions and neglects the contribution of nascent adhesions and potentially some small focal complexes. Since the maturation of nascent adhesions and focal complexes into larger focal adhesions is an important event in migration, a more complete picture relating adhesive properties to migratory behavior can be formed if they are taken into account. Even with overestimation of the size of very small adhesions, cells cultured on three of the four nanopatterned surfaces formed significantly smaller adhesions compared to cells on non-patterned controls and a trend of increased adhesion size with increased pattern size was observed (Figure 3A–C). These results demonstrate the ability to tune the extent of adhesion site growth through modulation of nanopattern size.

Through visual inspection of the vinculin images, we observed that cells on nanopatterned surfaces displayed an increased number of smaller, more densely packed adhesions (number of adhesions per area) compared to cells on controls (Figure 2). To gain insight into how limiting adhesion site growth influenced the number of adhesions formed, the average number of adhesions per cell was measured (Figure 3D). A nanopattern-size-dependent decay in the average number of adhesions formed was observed, leading to distinct clusters in the data (Figure 3D). The first cluster was composed of cells cultured on sub-100 nm sized patterns that formed ∼2100 adhesions per cell, followed by cells on larger nanopatterns, 222–405 nm, that formed ∼1600 adhesions per cell (Figure 3D). Finally, cells cultured on nonpatterned controls, with no restrictions on adhesion site growth, formed ∼1000 adhesions per cell (Figure 3D). We also observed slightly impaired spreading in cells cultured on the sub-100 nm sized patterns, and to account for differences in spreading, the adhesion site density (number of adhesions per area) was quantified and the data normalized to the spread area of a typical cell on a nonpatterned control surface (5000 μm^2) (Figure 3E). The trend was similar to the number of adhesions formed (Figure 3D), but a more pronounced decay in adhesion site density with increased nanopattern size was observed (Figure 3E). The adhesion site density decayed from ∼3235 to ∼795 adhesions/5000 μm^2 for cells on the 0300B and 25Au surfaces, respectively (Figure 3E). These results demonstrate that limiting adhesion site growth induced cells to form an increased

DOI: 10.1021/am508906f
ACS Appl. Mater. Interfaces 2015, 7, 4390–4400

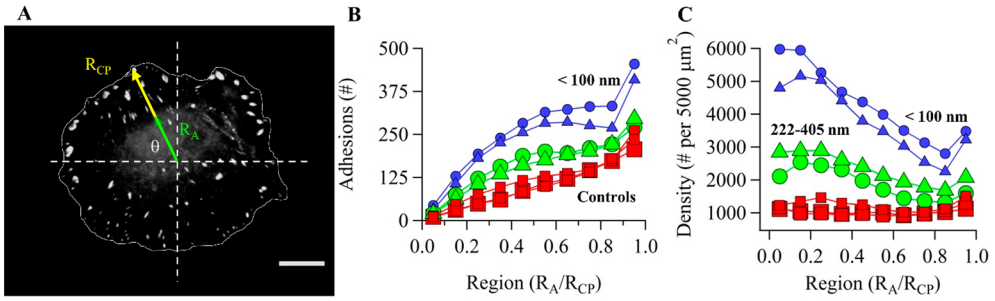

Figure 4. Limiting adhesion site growth induces a redistribution of adhesion sites. Intracellular distribution of vinculin-containing adhesions was measured from immunofluorescent images of HUVECs cultured on nanopatterned and control surfaces. The increased number and density of adhesions formed by cells on nanopatterned surfaces displayed in Figure 3 coincided with more adhesions located in the interior of the cells. (A) This observation was quantified by mapping the ratiometric location of each adhesion site. The distance from the cell centroid to each adhesion (R_A: green arrow) at a given angle (θ) was divided by the distance from the cell centroid to the cell periphery (R_{CP}: yellow arrow) at the same θ. (B, C) The cell was divided into ten regions, and the ratiometric location (R_A/R_{CP}) for each adhesion was mapped; a value of 0 corresponds to an adhesion at the cell centroid and 1 to an adhesion at the cell periphery. (B) A trend of increased numbers of adhesions from the cell center to the cell periphery was observed for cells on both nanopatterned and control surfaces. (B) A nanopattern size induced division was observed where cells cultured on (blue symbols in B) sub-100 nm sized patterns displayed similar adhesion site distributions, cells cultured on (green symbols in B) nanopatterns 222−405 nm in size were similar, and cells on (red in B) nonpatterned controls displayed similar distributions. (C) The nanopattern sized induced divisions in the adhesion site distribution were more pronounced in the adhesion site density data. (A) Scale bar = 20 μm.

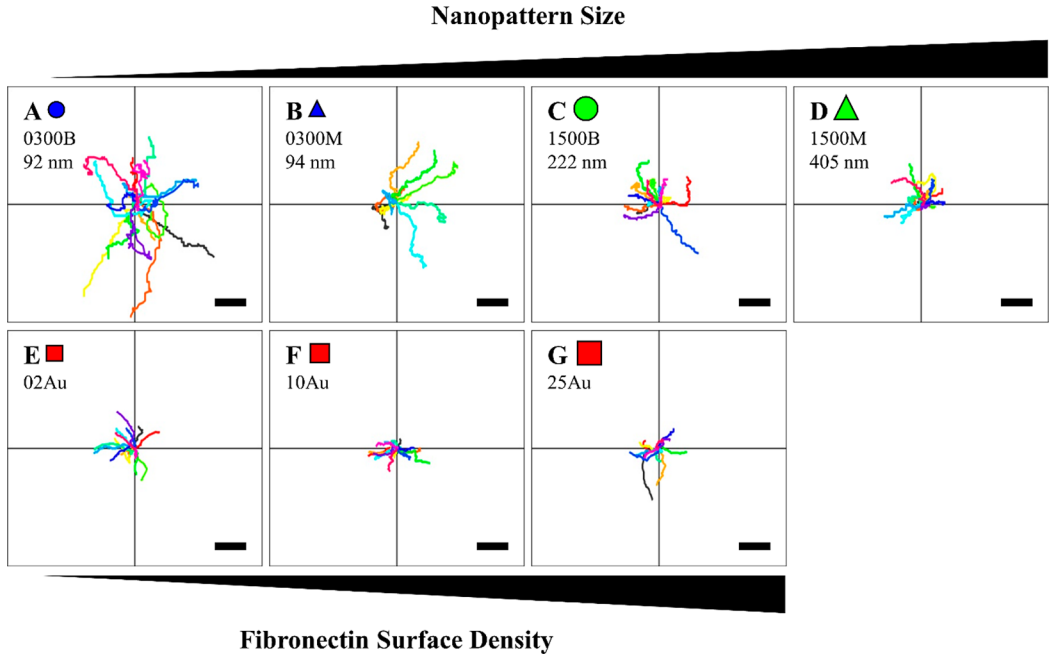

Figure 5. Limiting adhesion site growth induces enhanced migration. (A−G) Migration paths of HUVECs cultured on (A−D) nanopatterned and (E−G) control surfaces. HUVECs were cultured on the surfaces and imaged with time-lapse phase-contrast microscopy for 90 min. The centroid of each cell was measured at 1 min intervals and plotted to create the migration paths. HUVECs cultured on nanopatterned surfaces displayed enhanced migration compared to cells on control surfaces (compare top row to bottom row). The extent of migration enhancement was dependent on nanopattern size; as the nanopattern size increased migration decreased. (A−G) Scale bar = 25 μm.

number of smaller, more densely packed adhesions similar to what has been observed in cells cultured on elastic surfaces.[16,45,46]

3.3. Limiting Adhesion Site Growth Induced a Change in the Distribution of Adhesion Sites. Differences observed in the number and density of adhesions between cells on nanopatterned and controls surfaces suggested that the distribution of adhesions throughout the cells may also differ. To quantify the distribution of adhesions, a ratiometric adhesion site mapping technique was developed (Figure 4A). The distance from the cell centroid to the cell periphery (R_{CP}) was measured at a given angle (θ) (yellow in Figure 4A), and the distance to the centroid of each adhesion site (R_A), at the same θ, was measured (green in Figure 4A). For each θ, the ratio R_A/R_{CP} provided a ratiometric determination of each adhesion site's location within the cell (Figure 4B,C). The process is equivalent to mapping the cell onto a circle of radius 1, with a value of 0 for adhesions at the cell center and 1 at the periphery.

Cells on all surfaces displayed an increased number of adhesions toward the periphery (Figure 4B), which is mostly a reflection of the linear increase in the area of a ring of constant width with radial distance. Cells on nonpatterned controls displayed a linear increase in the number of adhesions with

DOI: 10.1021/am508906f
ACS Appl. Mater. Interfaces 2015, 7, 4390−4400

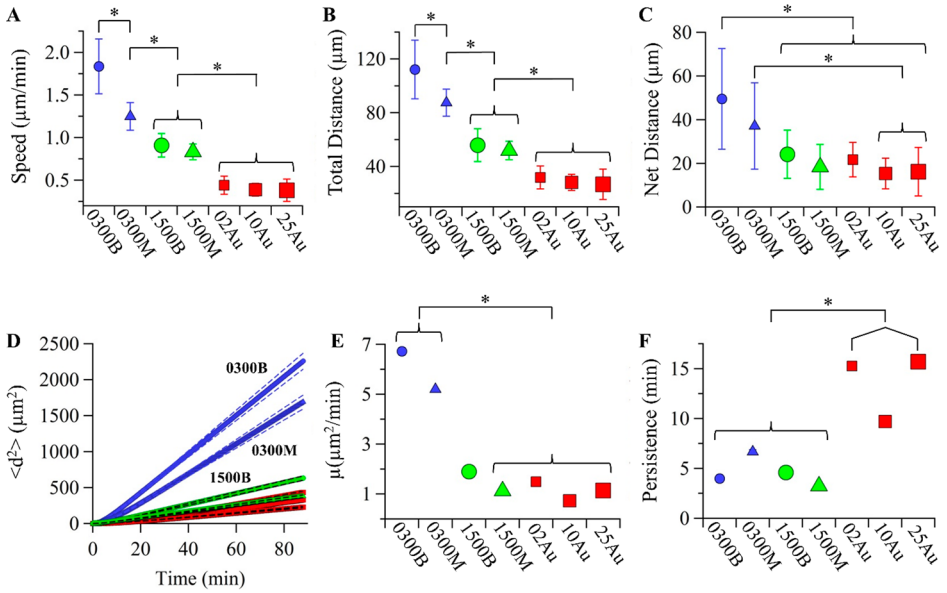

Figure 6. Characterization of HUVEC migration on nanopatterned and control surfaces. (A) Root-mean-square speed, average (B) total and (C) net distance traveled, (D) mean square displacement, (E) random motility coefficient, and (F) persistence time were determined from the migration paths in Figure 5. (A) Cells cultured on nanopatterned surfaces displayed significantly enhanced speed, and the average speed decreased as the nanopattern size increased. (B) HUVECs on nanopatterned surfaces traveled a significantly increased total distance compared with cells on control surfaces, and (C) those on sub-100 nm sized patterns (0300B and 0300 M surfaces) traveled significantly farther from their point of origin than cells on controls. (D) The mean square displacement versus time for cells migrating on control and nanopatterned surfaces. (D) Dashed black lines indicate upper and lower bounds for 90% confidence of the fits. (E) Cells migrating on sub-100 nm sized patterns displayed significantly increased diffusion and (F) cells on all of the nanopatterns displayed significantly decreased persistence time compared to cells on controls. Standard deviation bars for data points in E, F are of equal size or smaller than the symbols used to mark the data points. * indicates $p < 0.5$.

radial distance from the center (Figure 4B), indicating a constant density of adhesions over the spread area of the cell (Figure 4C). In contrast, cells on nanopatterned surfaces showed a linear increase in the number of adhesions only up to the middle of the cell with a higher slope (Figure 4B), indicating a higher density than controls and a higher density in the cell center (Figure 4C). Again, distinct clustering in the distribution data as a function of nanopattern size as observed in Figure 3 was also seen here.

One may speculate that if sustained force needs to be applied to adhesions through Rho-mediated actomyosin contraction to increase attachment area and adhesion maturation, then nanopatterned surfaces may prevent maturation by limiting the applied force. These results would then indicate the ability to tune the maturation level of adhesions by simply modulating adhesion site growth. Because small, nascent adhesions are more dynamic than larger, mature adhesions but can still apply relatively high traction forces for their size, limiting adhesion site growth should lead to highly dynamic cells that exhibit enhanced migration. This would be consistent with previous studies that have shown that preventing the formation of stable focal adhesions by manipulating integrin spacing induces highly dynamic adhesions that impair cell spreading and induce increased migration.[29] The following data demonstrates that limiting adhesion site growth has a significant impact on cell dynamics and migration.

3.4. Migration Speed, Mobility, and Persistence Are Influenced by Adhesion Site Size. To investigate the influence of limiting adhesion site growth on cell migration, HUVECs were sparsely seeded on nanopatterned and control surfaces and monitored 24 h postseeding in a climate-controlled chamber. Phase-contrast images were acquired at 1 min intervals for 90 min to generate cell migration paths (Figure 5). The path contours indicated that cells on nanopatterned surfaces, especially those on sub-100 nm sized patterns (Figure 5A,B), migrated faster and appeared more persistent than cells on nonpatterned controls (Figure 5E−G). An analysis of the time-lapse data indicated that cells migrating on the smallest, 92 nm patterns, had the highest speed of 1.83 ± 0.32 μm/min, that decreased to 0.83 ± 0.09 μm/min as the nanopattern size increased to 405 nm, a 4.8-fold and 2.1-fold increase, respectively, over cells on nonpatterned controls which only migrated at 0.38 ± 0.13 μm/min (Figure 6A).

Consistent with these differences in speed, cells traveled a contour distance of 112, 87, 56, and 52 μm on 0300B, 0300M, 1500B, and 1500 M surfaces, respectively, compared to only 32, 28, and 27 μm for cells on 2Au, 10Au, and 25Au control surfaces (Figure 6B). Cellular migration was random as the net distance (Figure 6C) and mean square displacement indicated (Figure 6D). The random motility coefficient (μ), the equivalent of diffusivity, was 5 to 7 times higher for cells migrating on sub-100 nm sized patterns and mostly constant for cells on all other surfaces (Figure 6E). Consequently, the directional persistence time was similar on the nanopatterns and significantly lower compared to controls (Figure 6F). This inverse relationship between speed and persistence time with slower cells showing increased persistence time has previously been reported.[47] Although cells migrating on nanopatterned surfaces displayed decreased persistence time, they migrated much faster and displayed a persistence length of 7.82 μm on sub-100 nm sized pattern, which was longer than cells on larger nanopatterns and controls with persistence lengths of 3.43 and 5.48 μm, respectively. Consequently, while cells on all of the nanopatterned surfaces were significantly faster and traveled a longer contour length compared to those on control surfaces, only cells exhibiting an increased random motility coefficient

DOI: 10.1021/am508906f
ACS Appl. Mater. Interfaces 2015, 7, 4390−4400

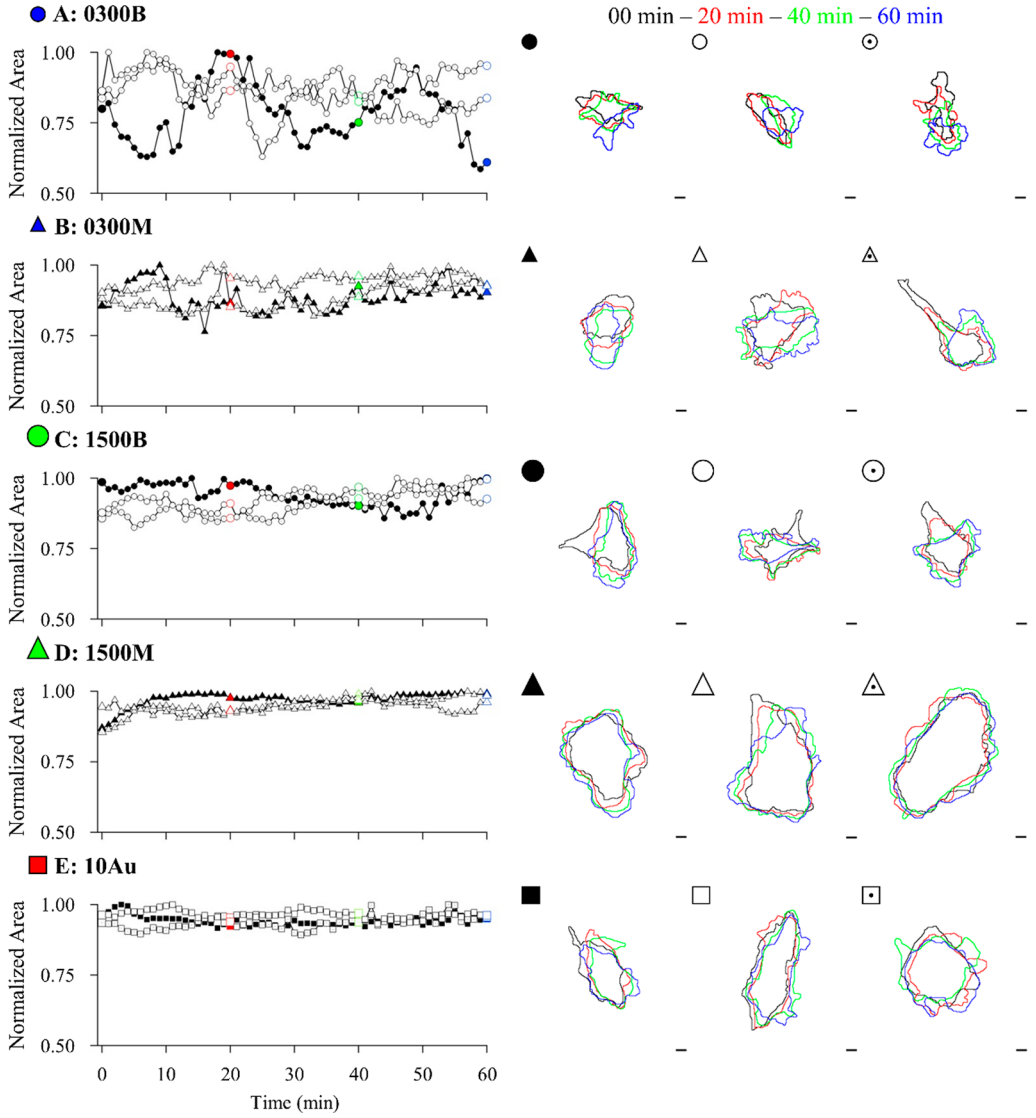

Figure 7. Limiting adhesion site growth induces dynamic cell behavior during migration. Cell spread area was measured for cells migrating on the indicated surfaces at 1 min intervals for 1 h. (A–E) The spread area at each time point was normalized to the maximum area measured during the 1 h observation window and plotted versus time. (A) Cells migrating on the smallest nanopatterns were extremely dynamic and displayed up to a 41% change in area over only a 10 min time period. (A–E) The changes in spread area with time and overall cell dynamics decreased as the nanopattern size increased. Outlines of the cells analyzed at t = 0, 20, 40, and 60 min are displayed in the right column. The symbols in the upper left corner of the composite cell outline images correspond to the data points in the left column. Scale bars = 20 μm.

displayed significantly increased start-to-end distances (Figure 6C) and persistence lengths. These results demonstrate that limiting the extent of adhesion site growth induced a significant increase in cell speed, but only the sub-100 nm sized patterns influenced the diffusive behavior of migrating cells. These results indicate that migratory behavior can be tuned by varying the size of the FN nanopatterns and that an inverse relationship between nanopattern size and migration exists where cells on smaller nanopatterns exhibit increased migratory behavior.

These differences in migratory behavior between cells on nanopatterned and control surfaces were reflected in the cell spreading dynamics, as represented by changes in cell shape and spreading over time (Figure 7). Cells migrating on sub-100 nm sized patterns were much more dynamic and displayed drastic fluctuations in cell shape and spreading during migration (Figure 7A,B) compared to cells on larger nanopatterns (Figure 7C,D) and nonpatterned controls (Figure 7E). Cells migrating on 0300B surfaces displayed area fluctuations as large as 41% over a 10 min interval that steadily decreased to 24%, 18%, 15%, and 11% for cells on the 0300M, 1500B, 1500M, and 10Au surfaces, respectively (Figure 7). These drastic differences in cell morphology were due to highly increased lamellipodia formation and retraction and were not associated with filopodia extensions. Such increased cell dynamics due to limited adhesion site growth is consistent with the predominance of short-lived immature adhesions and absence of stabilizing mature, focal adhesions.

4. DISCUSSION

Two distinct modes of cell migration have been observed in cells on two-dimensional, planar surfaces. Many mammalian cells including fibroblasts, endothelial cells, and smooth muscle cells utilize an extension–retraction mode of migration characterized by protrusion at the leading edge, retraction of the cell body, and release at the trailing end. Cells utilizing this mode of migration display slow migration at ~0.5 μm/min. On

DOI: 10.1021/am508906f
ACS Appl. Mater. Interfaces 2015, 7, 4390–4400

the other hand, some cancer cells such as HT1080 fibrosarcoma cells utilize a gliding mode of migration that is characterized by the presence of a large lamellipodia, a very small or negligible trailing end, and the presence of only small, immature adhesions.[48] Cells utilizing this mode of migration exhibit much higher speed at ∼1.6 μm/min.[48] The migration rates of these cells can be significantly decreased by enhancing cytoskeletal linkage of adhesion sites through activation of tensin genes, an adaptor protein that increases cytoskeletal linkage to adhesions and induces adhesion site growth.[49] While cells exhibiting either mode of motility utilize the same intracellular machinery to generation traction forces to propel the cell forward there are subtle differences in how the propulsive forces are generated. Cells utilizing the extension-retraction mode of motility rely heavily on the generation of myosin-mediated traction forces exerted at focal complexes and focal adhesions whereas cells exhibiting gilding migration rely on traction force generated by nascent adhesions that emanates from their interaction with treadmilling actin in the highly cross-linked, dense actin network in the lamellipodium independent of myosin II activity.[12] Although, highly migratory cells on sub-100 nm sized patterns in this study did not exhibit gliding style migration, they did display predominately small adhesions, a broad lamellipodium, negligible trailing end, and a speed similar to fibrosarcoma cells indicating that some of these properties were induced by preventing adhesion growth.

Knowing that small, immature adhesions can generate relatively high[4] but short-lived[6] traction forces compared to longer-lived, larger, mature adhesions, suggests a model in which limiting adhesion site growth induces enhanced migration by reducing the rate-limiting step of adhesion site disassembly in an adhesion site size-dependent manner. Evidence for this model is provided by the significantly increased speed, mobility, and cell dynamics observed in cells on sub-100 nm sized patterns that formed the smallest adhesion sites. As adhesion site growth was allowed to increase using 220−450 nm sized patterns, the cells still displayed enhanced speed compared to controls, but their dynamics began to slow. As all restrictions on adhesion site growth were lifted, cells on control surfaces displayed much slower speed and dynamics. In contrast to mature focal adhesions, which are much more stable and have a slower turnover rate, small immature adhesions are known to have a decreased lifetime,[15] in agreement with these findings. The observations here can be summarized in the relationship between cell speed and adhesion site size, which shows an exponential decay in cell speed as a function of increasing adhesion size (Figure 8).

Several groups have shown that adhesion site disassembly can be a rate-limiting step in migration[9,10,15,48] and that smaller adhesions are more dynamic and less stable.[29] The results presented here imply that preventing the formation of large focal adhesions by restricting adhesion site growth leads to increased cell dynamics and subsequently enhanced migration by avoiding the rate-limiting step of disassembling large mature adhesions, adding a new perspective on the phenomena observed in highly motile cancer cells. These findings are supported by the idea that a minimum adhesion area is needed for stable adhesion formation through balancing cytoskeletal generated forces with adhesion forces.[35] This logic implies that limiting adhesion site growth to small, immature adhesions results in the generation of propulsive forces while eliminating the rate-limiting step of adhesion site disassembly although future studies quantifying adhesion site turnover rates as a function of nanopattern size need to be performed for validation. Similar observations to those presented here have been observed in cells with impaired integrin clustering,[29] in cells on elastic substrates,[16] and in cells on nanopatterned surfaces.[36] Cells with impaired integrin clustering exhibited highly dynamic adhesions, less stress fiber formation, and increased lamellipodial dynamics which led to impaired spreading and increased migration[36] similar to cells on flexible substrates that displayed reduced cell spreading, increased adhesion dynamics, and subsequently a 6-fold increase in lamellapodial ruffling and 9-fold increase in speed compared to cells on stiff substrates.[16] Interestingly, these cells also exhibited smaller, more dynamic punctate adhesions throughout the cell body,[16,45,46] similar to the adhesive states observed in cells cultured on nanopatterned surfaces in this study.

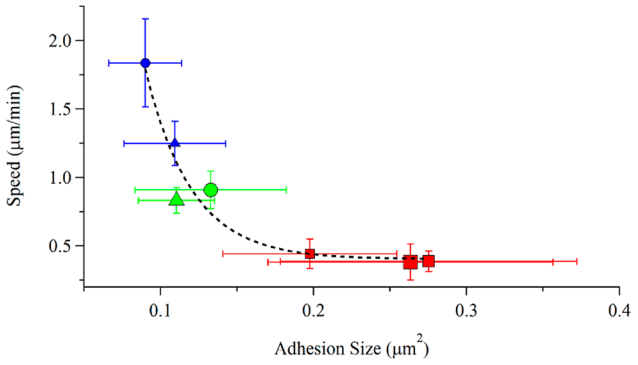

Figure 8. There is an exponential decay in cell speed as adhesion site size increases. An exponential decay in cell speed was observed with increased adhesion site size, independent of the total adhesion area. The results indicate that restricting adhesion site growth with sub-100 nm sized nanopatterns induced highly migratory cell behavior characterized by significantly increased cell spreading dynamics, speed, and mobility. As the adhesion site size was allowed to slightly increase, as induced in cells cultured on 222−405 nm sized patterns, the extent of migratory enhancement slightly decreased and coincided with decreased spreading dynamics, speed, and mobility. Finally, as all restrictions imposed on adhesion site growth were lifted with control surfaces, the cells displayed significantly decreased speed that coincided with decreased spreading dynamics and mobility. It has previously been shown that large focal adhesions at the cell periphery have much longer life times than small nascent adhesions or focal complexes. We speculate that limiting adhesion site growth to just that of short-lived nascent adhesions and focal complexes lifts the rate-limiting step of focal adhesion disassembly, resulting in highly migratory cell behavior.

While this study focused on the migration of single cells it has been shown that nanopatterned substrates can influence collective cell migration.[25] HeLa cells cultured on homogeneous, nonpatterned surfaces display collective migration mediated by n-cadherin in cell−cell contacts.[25] When cultured on nanopatterned substrates that limit integrin spacing to 57 nm, n-cadherin was downregulated, thereby abolishing collective migration and inducing single cell migration at ∼2.5-fold higher speed, indicating an environmental influence on cancer cell migration.[25] Taken together, the results presented here provide insight into how subtle changes in environmental cues, such as ECM organization, can significantly impact cell behavior.

DOI: 10.1021/am508906f
ACS Appl. Mater. Interfaces 2015, 7, 4390−4400

5. CONCLUSIONS

The work presented here provides a platform for investigating adhesion maturation with unprecedented control and without the use of chemicals that perturb cytoskeletal function to revert maturation to earlier states.[50] Furthermore, the results provide insight into what roles adhesions play during cell motility. We show that suppression of large adhesion site formation leads to enhanced cell migration, up to 4.8-fold faster, thereby indicating that disassembly of large, mature adhesions of motile cells may be a rate-limiting step in migration.

■ ASSOCIATED CONTENT

Supporting Information

Additional information as noted in the text. This material is available free of charge via the Internet at http://pubs.acs.org.

■ AUTHOR INFORMATION

Corresponding Author

*E-mail: jhslater@udel.edu.

Present Address

[ψ]Department of Biomedical Engineering, University of Delaware, Newark, DE, 19716.

Notes

The authors declare no competing financial interest.

■ ACKNOWLEDGMENTS

The authors acknowledge the support of NIH grants 1R21EB003038-01 and 5R21EB003038-02 to W.F. J.H.S. was supported by a NSF GRFP.

■ REFERENCES

(1) Huttenlocher, A.; Sandborg, R. R.; Horwitz, A. F. Adhesion in Cell Migration. *Curr. Opin. Cell Biol.* **1995**, *7*, 697−706.

(2) Hynes, R. O. Integrins - Versatility, Modulation, and Signaling in Cell-Adhesion. *Cell* **1992**, *69*, 11−25.

(3) Brinkerhoff, C. J.; Linderman, J. J. Integrin Dimerization and Ligand Organization: Key Components in Integrin Clustering for Cell Adhesion. *Tissue Eng.* **2005**, *11*, 865−876.

(4) Beningo, K. A.; Dembo, M.; Kaverina, I.; Small, J. V.; Wang, Y. L. Nascent Focal Adhesions Are Responsible for the Generation of Strong Propulsive Forces in Migrating Fibroblasts. *J. Cell Biol.* **2001**, *153*, 881−887.

(5) Webb, D. J.; Donais, K.; Whitmore, L. A.; Thomas, S. M.; Turner, C. E.; Parsons, J. T.; Horwitz, A. F. Fak-Src Signalling through Paxillin, Erk and Mlck Regulates Adhesion Disassembly. *Nat. Cell Biol.* **2004**, *6*, 154−161.

(6) Zaidel-Bar, R.; Ballestrem, C.; Kam, Z.; Geiger, B. Early Molecular Events in the Assembly of Matrix Adhesions at the Leading Edge of Migrating Cells. *J. Cell Sci.* **2003**, *116*, 4605−4613.

(7) Zaidel-Bar, R.; Cohen, M.; Addadi, L.; Geiger, B. Hierarchical Assembly of Cell-Matrix Adhesion Complexes. *Biochem. Soc. Trans.* **2004**, *32*, 416−420.

(8) Zaidel-Bar, R.; Milo, R.; Kam, Z.; Geiger, B. A Paxillin Tyrosine Phosphorylation Switch Regulates the Assembly and Form of Cell-Matrix Adhesions. *J. Cell Sci.* **2007**, *120*, 137−148.

(9) Franco, S. J.; Rodgers, M. A.; Perrin, B. J.; Han, J. W.; Bennin, D. A.; Critchley, D. R.; Huttenlocher, A. Calpain-Mediated Proteolysis of Talin Regulates Adhesion Dynamics. *Nat. Cell Biol.* **2004**, *6*, 977−983.

(10) Chen, W. T. Mechanism of Retraction of the Trailing Edge During Fibroblast Movement. *J. Cell Biol.* **1981**, *90*, 187−200.

(11) Tan, J. L.; Tien, J.; Pirone, D. M.; Gray, D. S.; Bhadriraju, K.; Chen, C. S. Cells Lying on a Bed of Microneedles: An Approach to Isolate Mechanical Force. *Proc. Natl. Acad. Sci. U. S. A.* **2003**, *100*, 1484−1489.

(12) Choi, C. K.; Vicente-Manzanares, M.; Zareno, J.; Whitmore, L. A.; Mogilner, A.; Horwitz, A. R. Actin and Alpha-Actinin Orchestrate the Assembly and Maturation of Nascent Adhesions in a Myosin II Motor-Independent Manner. *Nat. Cell Biol.* **2008**, *10*, 1039−1050.

(13) Reinhart-King, C. A.; Dembo, M.; Hammer, D. A. Endothelial Cell Traction Forces on RGD-Derivatized Polyacrylamide Substrata. *Langmuir* **2003**, *19*, 1573−1579.

(14) Lo, C. M.; Wang, H. B.; Dembo, M.; Wang, Y. L. Cell Movement Is Guided by the Rigidity of the Substrate. *Biophys. J.* **2000**, *79*, 144−152.

(15) Giannone, G.; Ronde, P.; Gaire, M.; Haiech, J.; Takeda, K. Calcium Oscillations Trigger Focal Adhesion Disassembly in Human U87 Astrocytoma Cells. *J. Biol. Chem.* **2002**, *277*, 26364−26371.

(16) Pelham, R. J.; Wang, Y. L. Cell Locomotion and Focal Adhesions Are Regulated by Substrate Flexibility. *Proc. Natl. Acad. Sci. U. S. A.* **1997**, *94*, 13661−13665.

(17) Shroff, H.; Galbraith, C. G.; Galbraith, J. A.; Betzig, E. Live-Cell Photoactivated Localization Microscopy of Nanoscale Adhesion Dynamics. *Nat. Methods* **2008**, *5*, 417−423.

(18) Slater, J. H.; Miller, J. S.; Yu, S. S.; West, J. L. Fabrication of Multifaceted Micropatterned Surfaces with Laser Scanning Lithography. *Adv. Funct. Mater.* **2011**, *21*, 2876−2888.

(19) Théry, M. Micropatterning as a Tool to Decipher Cell Morphogenesis and Functions. *J. Cell Sci.* **2010**, *123*, 4201−13.

(20) Mahmud, G.; Campbell, C. J.; Bishop, K. J. M.; Komarova, Y. A.; Chaga, O.; Soh, S.; Huda, S.; Kandere-Grzybowska, K.; Grzybowski, B. A. Directing Cell Motions on Micropatterned Ratchets. *Nat. Phys.* **2009**, *5*, 606−612.

(21) Doyle, A. D.; Wang, F. W.; Matsumoto, K.; Yamada, K. M. One-Dimensional Topography Underlies Three-Dimensional Fibrillar Cell Migration. *J. Cell Biol.* **2009**, *184*, 481−490.

(22) Xia, N.; Thodeti, C. K.; Hunt, T. P.; Xu, Q. B.; Ho, M.; Whitesides, G. M.; Westervelt, R.; Ingber, D. E. Directional Control of Cell Motility through Focal Adhesion Positioning and Spatial Control of Rac Activation. *FASEB J.* **2008**, *22*, 1649−1659.

(23) Kandere-Grzybowska, K.; Campbell, C. J.; Mahmud, G.; Komarova, Y.; Soh, S.; Grzybowski, B. A. Cell Motility on Micropatterned Treadmills and Tracks. *Soft Matter* **2007**, *3*, 672−679.

(24) Liu, D.; Abdullah, C. A. C.; Sear, R. P.; Keddie, J. L. Cell Adhesion on Nanopatterned Fibronectin Substrates. *Soft Matter* **2010**, *6*, 5408−5416.

(25) Shimizu, Y.; Boehm, H.; Yamaguchi, K.; Spatz, J. P.; Nakanishi, J. A Photoactivatable Nanopatterned Substrate for Analyzing Collective Cell Migration with Precisely Tuned Cell-Extracellular Matrix Ligand Interactions. *PLoS One* **2014**, *9*, e91875.

(26) Deeg, J. A.; Louban, I.; Aydin, D.; Selhuber-Unkel, C.; Kessler, H.; Spatz, J. P. Impact of Local versus Global Ligand Density on Cellular Adhesion. *Nano Lett.* **2011**, *11*, 1469−1476.

(27) Selhuber-Unkel, C.; Erdmann, T.; Lopez-Garcia, M.; Kessler, H.; Schwarz, U. S.; Spatz, J. P. Cell Adhesion Strength Is Controlled by Intermolecular Spacing of Adhesion Receptors. *Biophys. J.* **2010**, *98*, 543−551.

(28) Arnold, M.; Schwieder, M.; Blummel, J.; Cavalcanti-Adam, E. A.; Lopez-Garcia, M.; Kessler, H.; Geiger, B.; Spatz, J. P. Cell Interactions with Hierarchically Structured Nano-Patterned Adhesive Surfaces. *Soft Matter* **2009**, *5*, 72−77.

(29) Cavalcanti-Adam, E. A.; Volberg, T.; Micoulet, A.; Kessler, H.; Geiger, B.; Spatz, J. P. Cell Spreading and Focal Adhesion Dynamics Are Regulated by Spacing of Integrin Ligands. *Biophys. J.* **2007**, *92*, 2964−2974.

(30) Arnold, M.; Cavalcanti-Adam, E. A.; Glass, R.; Bluemmel, J.; Eck, W.; Kantlehner, M.; Kessler, H.; Spatz, J. P. Activation of Integrin Function by Nanopatterned Adhesive Interfaces. *ChemPhysChem* **2004**, *5*, 383−388.

(31) Slater, J. H.; Frey, W. Nanopatterning of Fibronectin and the Influence of Integrin Clustering on Endothelial Cell Spreading and Proliferation. *J. Biomed. Mater. Res., Part A* **2008**, *87A*, 176−195.

(32) Malmström, J.; Christensen, B.; Jakobsen, H. P.; Lovmand, J.; Foldbjerg, R.; Sørensen, E. S.; Sutherland, D. S. Large Area Protein

DOI: 10.1021/am508906f
ACS Appl. Mater. Interfaces 2015, 7, 4390−4400

Patterning Reveals Nanoscale Control of Focal Adhesion Development. *Nano Lett.* **2010**, *10*, 686−694.
(33) Dalby, M. J.; Riehle, M. O.; Sutherland, D. S.; Agheli, H.; Curtis, A. S. G. Fibroblast Response to a Controlled Nanoenvironment Produced by Colloidal Lithography. *J. Biomed. Mater. Res., Part A* **2004**, *69A*, 314−322.
(34) Lutz, R.; Pataky, K.; Gadhari, N.; Marelli, M.; Brugger, J.; Chiquet, M. Nano-Stenciled RGD-Gold Patterns That Inhibit Focal Contact Maturation Induce Lamellipodia Formation in Fibroblasts. *PLoS One* **2011**, *6*, e25459.
(35) Coyer, S. R.; Singh, A.; Dumbauld, D. W.; Calderwood, D. A.; Craig, S. W.; Delamarche, E.; García, A. J. Nanopatterning Reveals an Ecm Area Threshold for Focal Adhesion Assembly and Force Transmission That Is Regulated by Integrin Activation and Cytoskeleton Tension. *J. Cell Sci.* **2012**, *125*, 5110−5123.
(36) Westcott, N. P.; Lou, Y.; Muth, J. F.; Yousaf, M. N. Patterned Hybrid Nanohole Array Surfaces for Cell Adhesion and Migration. *Langmuir* **2009**, *25*, 11236−11238.
(37) Chinga, G.; Johnsen, P. O.; Dougherty, R.; Berli, E. L.; Walter, J. Quantification of the 3D Microstructure of SC Surfaces. *J. Microsc. (Oxford, U. K.)* **2007**, *227*, 254−265.
(38) Dikeman, D. A.; Rivera Rosado, L. A.; Horn, T. A.; Alves, C. S.; Konstantopoulos, K.; Yang, J. T. Alpha4 Beta1-Integrin Regulates Directionally Persistent Cell Migration in Response to Shear Flow Stimulation. *Am. J. Physiol.: Cell Physiol.* **2008**, *295*, C151−159.
(39) Keselowsky, B. G.; Collard, D. M.; Garcia, A. J. Integrin Binding Specificity Regulates Biomaterial Surface Chemistry Effects on Cell Differentiation. *Proc. Natl. Acad. Sci. U. S. A.* **2005**, *102*, 5953−5957.
(40) Keselowsky, B. G.; Collard, D. M.; Garcia, A. J. Surface Chemistry Modulates Focal Adhesion Composition and Signaling through Changes in Integrin Binding. *Biomaterials* **2004**, *25*, 5947−5954.
(41) Keselowsky, B. G.; Collard, D. M.; Garcia, A. J. Surface Chemistry Modulates Fibronectin Conformation and Directs Integrin Binding and Specificity to Control Cell Adhesion. *J. Biomed. Mater. Res., Part A* **2003**, *66A*, 247−259.
(42) Pirone, D. M.; Liu, W. F.; Ruiz, S. A.; Gao, L.; Raghavan, S.; Lemmon, C. A.; Romer, L. H.; Chen, C. S. An Inhibitory Role for Fak in Regulating Proliferation: A Link between Limited Adhesion and Rhoa-Rock Signaling. *J. Cell Biol.* **2006**, *174*, 277−288.
(43) Nelson, C. M.; Pirone, D. M.; Tan, J. L.; Chen, C. S. Vascular Endothelial-Cadherin Regulates Cytoskeletal Tension, Cell Spreading, and Focal Adhesions Stimulating Rhoa. *Mol. Biol. Cell* **2004**, *15*, 2943−2953.
(44) Zamir, E.; Katz, B. Z.; Aota, S.; Yamada, K. M.; Geiger, B.; Kam, Z. Molecular Diversity of Cell-Matrix Adhesions. *J. Cell Sci.* **1999**, *112*, 1655−1669.
(45) Discher, D. E.; Janmey, P.; Wang, Y. L. Tissue Cells Feel and Respond to the Stiffness of Their Substrate. *Science* **2005**, *310*, 1139−1143.
(46) Deroanne, C. F.; Lapiere, C. M.; Nusgens, B. V. In Vitro Tubulogenesis of Endothelial Cells by Relaxation of the Coupling Extracellular Matrix-Cytoskeleton. *Cardiovasc. Res.* **2001**, *49*, 647−658.
(47) Lauffenburger, D. A.; Horwitz, A. F. Cell Migration: A Physically Integrated Molecular Process. *Cell* **1996**, *84*, 359−369.
(48) Paku, S.; Tovari, J.; Lorincz, Z.; Timar, F.; Dome, B.; Kopper, L.; Raz, A.; Timar, J. Adhesion Dynamics and Cytoskeletal Structure of Gliding Human Fibrosarcoma Cells: A Hypothetical Model of Cell Migration. *Exp. Cell Res.* **2003**, *290*, 246−253.
(49) Rodrigue, C. M.; Porteu, F.; Navarro, N.; Bruyneel, E.; Bracke, M.; Romeo, P. H.; Gespach, C.; Garel, M. C. The Cancer Chemopreventive Agent Resveratrol Induces Tensin, a Cell-Matrix Adhesion Protein with Signaling and Antitumor Activities. *Oncogene* **2005**, *24*, 3274−3284.
(50) Alexandrova, A. Y.; Arnold, K.; Schaub, S.; Vasiliev, J. M.; Meister, J. J.; Bershadsky, A. D.; Verkhovsky, A. B. Comparative Dynamics of Retrograde Actin Flow and Focal Adhesions: Formation of Nascent Adhesions Triggers Transition from Fast to Slow Flow. *PLoS One* **2008**, *3*, 9.

DOI: 10.1021/am508906f
ACS Appl. Mater. Interfaces 2015, 7, 4390−4400